Edelweiss Applied Science and Technology
ISSN: 2576-8484
Vol. 9, No. 5, 346-367
2025
Publisher: Learning Gate
DOI: 10.55214/25768484.v9i5.6869

Elaboration and electrical characterization of electrodes made with Azadirachta indica's biochar and coconut shells' bio-pitch doped with TiO_2

N'Gissa ATTAH[1,2*], Damgou KONGNINE MANI[1,2], Essowè MOUZOU[1,2,3], Pali KPELOU[1,2]
[1]Department of Physics, Solar Energy Laboratory, University of Lomé, 01BP 1515, Togo; attahalexis13@gmail.com (N.A.).
[2]Regional Center of Excellence for Electricity Control, University of Lomé, 01BP 1515, Togo.
[3]Department of Physics, Laboratory of Physics of Materials and Semiconductor Components, University of Lomé, 01BP 1515, Togo.

Abstract: Composite electrodes based on carbon material have recently experienced the widest application in Plant Microbial Fuel Cells, owing to the advantageous properties that they possess. In general, the manufacturing process of these electrodes involves a complex procedure requiring high temperatures as well as the use of chemical solutions and fossil pitch as binders. This study aims to elaborate on cheap composite electrodes from neem charcoal used as an alternative carbon source and coconut shell bio-pitch used as an alternative binder to fossil coal tar. To enhance their electrical properties, a Biochar/TiO2 weight ratio of 0%, 20%, 33%, and 83% was developed. A homemade carbonizer with a lid suitable for collecting bio-oil and an electrode mold were designed and used in this study. Electrochemical impedance spectroscopy (EIS) technique was used to determine the electrical equivalent circuit of each sample, and the result was compared to the graphite recovered from a new Leclanché battery. The resistivity assessment revealed that the sample with 33% TiO2 has the lowest electrical resistivity (4.28 x 10-4 Ω.m) but is 9.3 times higher than that of graphite. The electrolytic resistivities of this sample are 1.37 Ω.cm2, compared with 1.602 Ω.cm2 for graphite. The charge transfer resistance obtained from the EIS measurements showed an electricity recovery capacity of samples containing 33% and 83% by weight of TiO2 is respectively 3.3 times and 59.8 times higher than that of graphite. This suggests that using biochar instead of fossil coal and repurposing coconut shells into bio-pitch instead of fossil pitch is a more sustainable and effective approach for producing high-performance electrodes.

Keywords: *Bio-pitch, Coconut shells, Electricity recovery capacity, Electrode, Neem charcoal, Plant microbial fuel cells.*

1. Introduction

Biofuel cells, particularly Plant Microbial Fuel cells, emerge as viable alternatives to traditional energy sources, exhibiting a greater degree of environmental responsibility. These cells are particularly environmentally friendly due to the fact that the materials utilized in their design are less harmful to the environment. These cells are based on the oxidation of nutrients (substrates) by microorganisms present in the root zone of the plant. The oxidation of the substrate releases electrons and H+ protons. These electrons are captured by the anode and subsequently flow through an external circuit to the cathode. The protons, in turn, traverse the soil to the cathode, where they contribute to the reduction of oxygen. The processes of charge transport, transfer, and reduction result in significant losses, leading to decreased biofuel cell performance.

In order to enhance the efficiency of biofuel cells, research has been conducted with the objective of reducing their internal resistance. To achieve this, improve soil conductivity, optimize the distance between electrodes [1-3] and explore electrode materials [4, 5]. In order to minimize electron losses, the materials utilized to manufacture electrodes must possess the following characteristics: high

History: Received: 7 February 2025; Revised: 22 April 2025; Accepted: 25 April 2025; Published: 5 May 2025
* Correspondence: attahalexis13@gmail.com

electrical conductivity, a substantial specific surface area, biocompatibility, chemical stability, a homogeneous interfacial surface, minimal charge transfer resistance, and adequate porosity for biofilm development [6]. In recent years, there has been an uptick in research focusing on alternative electrode materials. A significant body of research has employed carbon-based materials as electrodes for biofuel cells [7, 8]. Specifically, carbon brushes, carbon rods, graphite fabric, graphite felt, and activated carbon have all been used for this purpose. However, these materials are not without their drawbacks, including high cost and low conductivity.

The utilization of metals that are effective conductors, including platinum, lead, and iron, is also unsuitable due to environmental concerns and their substantial cost. The utilization of charcoal as an electrode material emerges as a promising alternative. According to several researchers, the incorporation of metal oxides, such as zinc oxide (ZnO), titanium oxide (TiO_2), and silver (Ag) nanoparticles, into charcoal can remarkably augment the conductivity and biocompatibility of bacteria within microbial fuel cells [5, 6, 9-12].

In the majority of instances, the use of binders such as fossil pitch, polymers, and chemical solutions is employed in the fabrication of electrodes [6, 13, 14]. These substances have been shown to have deleterious effects on the environment and to increase the electrical resistance of the electrodes. For instance, coal tar pitch has been identified as a significant contributor to carbon monoxide, sulfur monoxide, and polycyclic aromatic hydrocarbon emissions, which are recognized carcinogens [15].

This study aims to develop affordable electrodes that have a minimal environmental impact. To this end, charcoal derived from the carbonization of neem wood (Azadirachta indica A.) is utilized as a carbonaceous material. The use of bio-pitch from coconut shells (a byproduct of the agricultural industry) has been proposed as a substitute for fossil pitch, serving the role of a binder. To enhance the electrical properties of the samples, varying amounts of TiO_2 were incorporated by weight. The resulting samples' electrical characteristics were subsequently determined through the implementation of electrochemical impedance spectroscopy.

2. Materials and Methods

2.1. Materials

2.1.1. Carbonizer and Electrode Mold

The carbonizer employed for the carbonization of neem wood has been previously described by Kpelou, et al. [16] in the context of co-producing hot water by means of carbonizing teak wood. The same carbonizer was used in the present study to carbonize coconut shells, but with a modified lid to recover bio-oil. The cover, a 1.5 mm-thick sheet of metal, was meticulously crafted to ensure its integrity and functionality.

The device designed for the recovery of condensed gaseous compounds (bio-oil) consists of a conical lid (inverted funnel), the upper extremity of which is extended by a metal tube with a diameter of 3.6 cm. The upper section of the conical structure consists of two components: a metal component that is directly extended from the end of the conical structure and a PVC (polyvinyl chloride) pipe. The PVC component incorporates an elbow joint, which functions as a connection point for various pipe lengths within the chimney system. At the base of the elbow, there is an 8mm diameter hole through which the bio-oil is collected (Figure 1). The dimensions of the utilized PVC pipes for the chimney are 54 cm and 67.5 cm, respectively (Figure 1).

Edelweiss Applied Science and Technology
ISSN: 2576-8484
Vol. 9, No. 5: 346-367, 2025
DOI: 10.55214/25768484.v9i5.6869

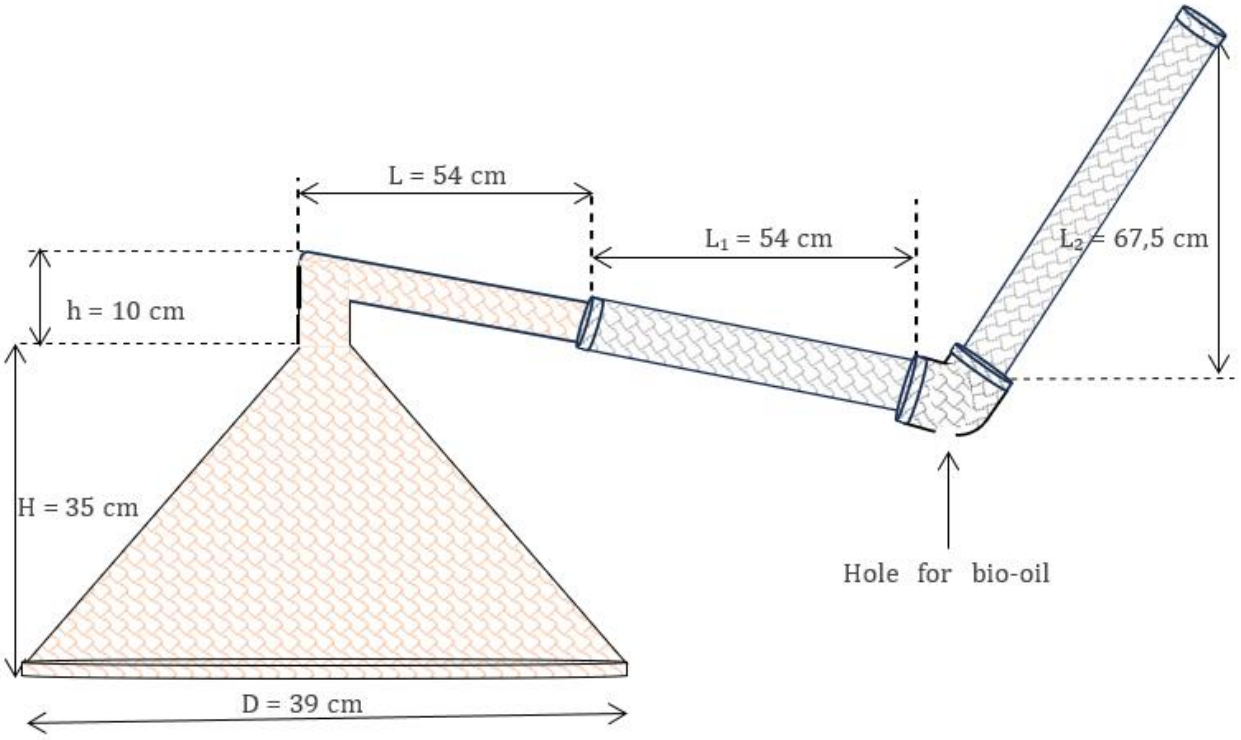

Figure 1.
Diagram of the carbonator cover for bio-oil production.

In our laboratory, an electrode mold was also designed for the fabrication of the electrodes. This mold consists of a metal cylinder with an external diameter of 5.49 cm, an internal diameter of 0.91 cm, and a height of 8.2 cm. Attached to the cylinder is a system of movable supports that carry a threaded piston. This mobile system is connected to the cylinder by two screws that allow for adjustment of the piston position during electrode molding and demolding (Figure 2).

Edelweiss Applied Science and Technology
ISSN: 2576-8484
Vol. 9, No. 5: 346-367, 2025
DOI: 10.55214/25768484.v9i5.6869

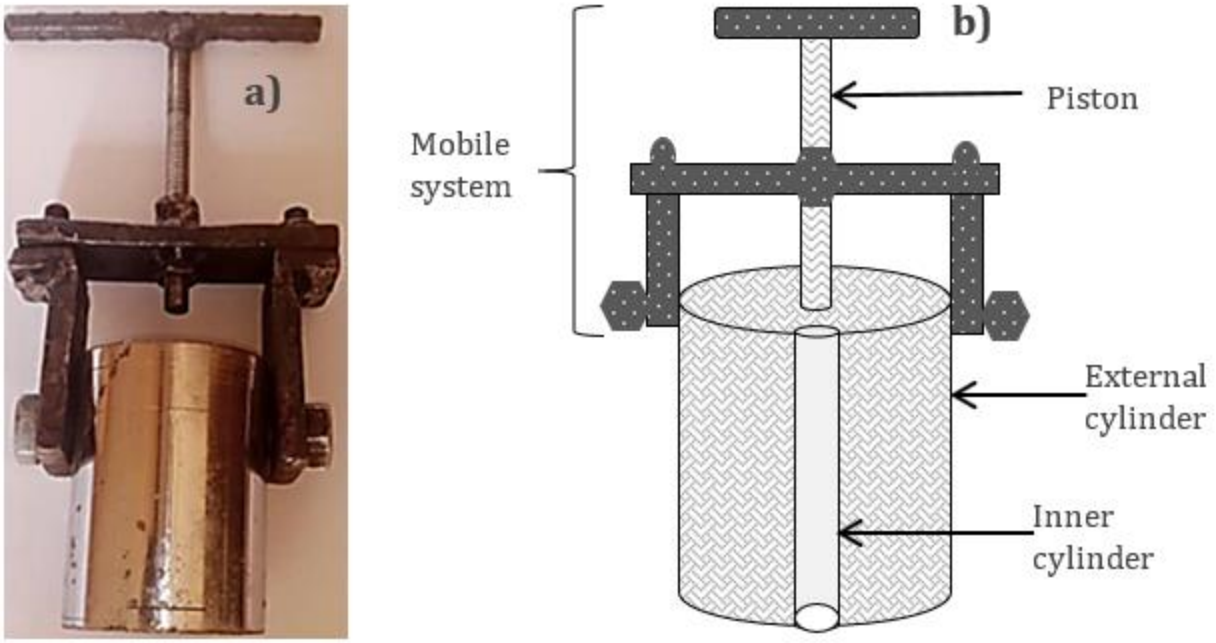

Figure 2.
Electrode mold: a) Photo; b) Schematic section.

2.1.2. Electrochemical Analyses

The CS350M EIS Potentiostat/Galvanostat is utilized to evaluate the redox and surface characteristics of electrode specimens. Electrochemical impedance spectroscopy (EIS) was performed in a conventional three-electrode setup comprising a reference electrode (AgCl/Ag), a platinum counter electrode, and a working electrode (the electrode being tested). The electrolyte utilized was a 1M sodium sulfate solution (Na_2SO_4). The EIS was conducted within a frequency range of 100 kHz to 100 mHz, with a voltage amplitude of 10 mV. Subsequent to the completion of the EIS, Nyquist and Bode plots were generated, and the electrochemical characteristics of each electrode were determined. However, analysis of the B/T (1:0) and B/T (4:1) electrodes was precluded due to their friability after heat treatment.

3. Methods

3.1. Samples Collection and Carbonization Technique

All of the raw materials utilized in this study were obtained from the Republic of Togo in West Africa. Coconut shells were obtained from small oil mills in Hahotoe (Lomé) and utilized in the production of bio-oil. Neem wood, sourced from Lomé City, was utilized for the production of charcoal. The technique for loading and igniting the biomass in the carbonizer was that described by Kpelou, et al. [16]. It is important to note that no gas flow was introduced during the carbonization processes.

3.2. Elaboration of Neem Charcoal

The carbonization of the neem wood was carried out using samples that were cut into parallelepiped shapes with dimensions of approximately 12x4x4 cm^3. The biomass charge utilized was consistent with the approach outlined by Kpelou, et al. [16]. A K-type thermocouple, connected to a data logger, was introduced at a height of 5 cm from the bottom of the carbonizer to monitor the temperature evolution. The process of carbonization was halted when the temperature within the carbonizer declined from 490°C to the minimum and then underwent an upward trend once more. The biochar obtained following

Edelweiss Applied Science and Technology
ISSN: 2576-8484
Vol. 9, No. 5: 346-367, 2025
DOI: 10.55214/25768484.v9i5.6869

the carbonization process was subsequently ignited in a stove. When the combustion became vigorous, characterized by the incandescence of all the pieces of biochar, the ignition process was halted. Subsequent to cooling, the ignited biochar pieces were selected based on their resistance values (lower than 30 Ω), which were measured using a 15XP-B multimeter. The neem charcoals that were selected were then ground in an aluminum mortar to a fine powder. This powder was subsequently sieved using a 50 µm mesh sieve.

3.3. Production of Biochar, Bio-Oil, And Bio-Pitch from Coconut Shells

The coconut shells were initially manually crushed in a small piece using a hammer. Subsequently, these pieces were subjected to sun-drying until it reached a constant weight. Thereafter, they were carbonized. The carbonization process of the coconut shells resulted in the production of biochar and bio-oil. The gaseous compounds that undergo carbonization and pass through the carbonizer chimney are converted into bio-oil. Neem wood was carbonized at a final temperature of 490 °C, while coconut shells were carbonized within the range of 414 °C and 466 °C. To enhance the bio-oil yield, the side holes of the carbonizer were plugged with fresh small wood, and kneaded soil was employed to seal the smoke leaks between the cylinder and its lid. The thermal profiles of the environment, as well as the surface and interior of the carbonizer, were recorded using thermocouples linked to a computer through a data logger. The appearance and flow rate of the bio-oil were closely monitored during a production process.

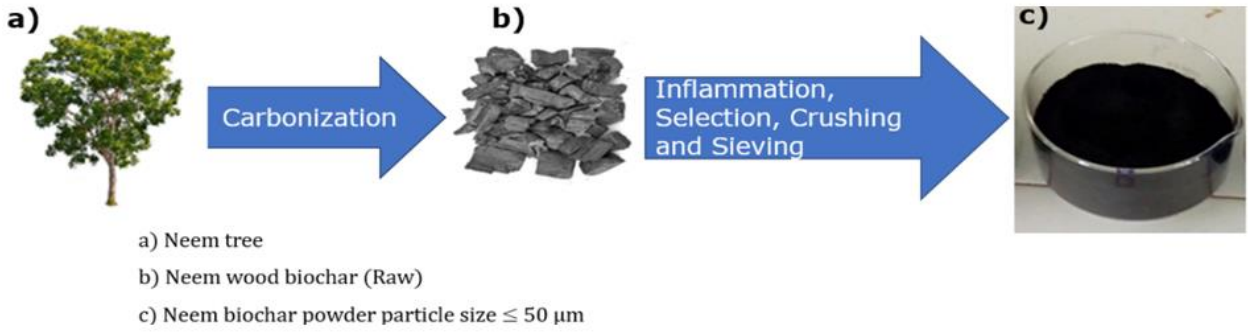

Figure 3.
Biochar Charcoal powder production process.

The density of the bio-oil solution was determined after its homogeneity was confirmed. To achieve this, the bio-oil solution was subjected to a 30-minute mixing process at a speed of 200 rpm using a magnetic stirrer (FOUR ES M10102002). The density of the bio-oil solution was subsequently determined by measuring the volume of the solution using a syringe and subsequently weighing the syringe before and after.

Using formula (1), the density was calculated:

$$\boldsymbol{Densit} = \frac{\boldsymbol{m_2 - m_1}}{\boldsymbol{V_{bio-oil}}} \quad (1)$$

Where $\boldsymbol{m_2}$is the mass of syringe with bio-oil; $\boldsymbol{m_1}$ is the mass of empty syringe and $\boldsymbol{V_{bio-oil}}$ is the volume of bio-oil taken by the syringe.

To obtain a bio-pitch suitable for the electrodes, the bio-oil was subjected to heat treatment with the same magnetic stirrer employed to ascertain the density of the bio-oil. Consequently, the heating of the stirrer was set to 105°C for a stirring speed of 200 revolutions per minute until a density of 1.3 g/cm^3 was obtained.

The mass yields of biochar, bio-oil and the volume ratio of bio-oil per kilogram of biomass were calculated using the following formulae (2) to (4).

Edelweiss Applied Science and Technology
ISSN: 2576-8484
Vol. 9, No. 5: 346-367, 2025
DOI: 10.55214/25768484.v9i5.6869

$$Y_{biochar} = \frac{m_{biochar}}{m_{biomass}} \times 100 \ (2)$$

Where $Y_{biochar}$is the biochar yield, $m_{biochar}$the mass of biochar and $m_{biomass}$ the initial mass of biomass to be carbonized.

$$Y_{bio-oil} = \frac{m_{bio-oil}}{m_{biomass}} \times 100 \ (3)$$

Where $Y_{bio-oil}$is the bio-oil yield, $m_{bio-oil}$the mass of bio-oil and $m_{biomass}$the mass of carbonized biomass.

$$R_{bio-oil} = \frac{V_{bio-oil}}{m_{biomass}} \times 100 \ (4)$$

Where $R_{bio-oil}$is the ratio of bio-oil, $V_{bio-oil}$ volume of bio-oil and $m_{biomasse}$ mass of carbonized biomass.

After being left to stand at room temperature in the laboratory for a week, the bio-oil produced was observed to exhibit three distinguishable phases. These phases included slightly dark supernatant phase at the top, a fairly voluminous lighter medium phase in the middle, and a darker phase at the bottom.

3.4. Elaboration of the Electrodes

The neem charcoals that were selected were ground in an aluminum mortar, resulting in a fine powder. Subsequently, the powder was subjected to a sieving process using a 50 µm mesh sieve. Four composite electrode samples were fabricated using 54.20% of this neem charcoal powder to which well-defined mass quantities of titanium oxide nanoparticles were added, and bio-pitch from coconut shells as a binder at a rate of 45.80% by weight (Figure 4).

The samples had a mean weight of approximately 4 g and were developed with varying weight ratios of TiO_2 nanoparticles: 0%, 20%, 33%, and 83%, respectively, identified as B/T (1:0); B/T (4:1); B/T (2:1); and B/T (1:5). The titanium oxide utilized in this study is P25, a product of Sigma-Aldrich, with a purity of 99.5%.

The samples were prepared by combining charcoal powders with bio-pitch to create a paste. The resultant paste was then introduced into the inner cylinder of the mold and compacted using a metal rod until it was fully filled, thereby completing the molding process. Subsequent to the molding process, the mobile system was adjusted to the position of demolding. The mold was placed horizontally and secured with a vice, and the piston was manually rotated. Small iron pieces, shaped like minutiae and matching the diameter of the piston but varying in size, were gradually inserted between the piston and the molded electrode. The pressure exerted by the piston on the electrode through these minutiae further enhanced the demolding process, causing the electrode to gradually exit the mold through the opposite side of the piston. The electrode production yield, defined as the percentage of demolded electrodes without breakage relative to the total number of molded electrodes, was calculated.

Edelweiss Applied Science and Technology
ISSN: 2576-8484
Vol. 9, No. 5: 346-367, 2025
DOI: 10.55214/25768484.v9i5.6869

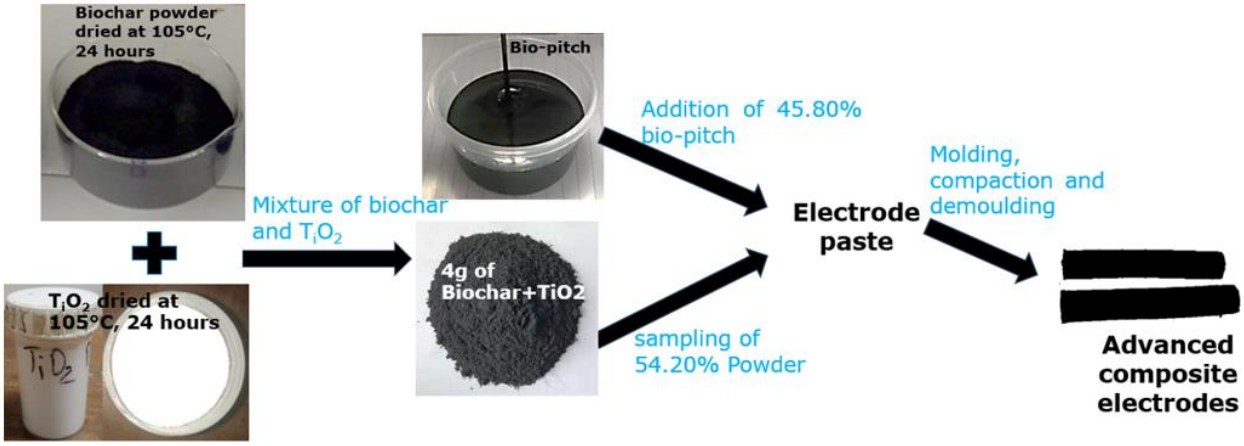

Figure 4.
Electrode production process.

The electrodes were exposed to ambient temperature for a period of eight days, thereby enabling natural drying processes to occur. Subsequent to this period, the electrodes were installed in an oven at 1 000°C for a duration of two hours within an inert atmosphere. Thereafter, the electrodes were removed from the oven at 45°C. The apparent density of each electrode, both before (raw electrode), as well as after the heat treatment (annealed electrode), was determined. The apparent density was calculated according to the ASTM D5502-00 standard [17] by determining the weight and dimensions of each electrode and subsequently calculating the apparent density.

The resistivity of each electrode was determined both before and after heat treatment using the four-point method. The resistivity of a graphite electrode recovered from a new Leclanché battery, which served as a reference in this study, was also measured by the same method. However, the forward resistivity of the B/T electrode (1:5) could not be determined using the four-point method due to its high resistance (0.664 MΩ). Consequently, the two-point method was employed for this measurement.

4. Results and Discussion

4.1. Biochar and bio-oil produced from coconut shells

The temperature distribution within a kiln during the carbonization process is a pivotal parameter that determines both the efficacy of the kiln and the quality of the final products. The carbonization process culminates in the production of biochar/charcoal and bio-oil. The neem charcoal obtained after this process was used as the carbon material for the elaboration of carbon-based electrodes. Given the low yield of bio-oil obtained by this carbonization process, a secondary process was necessary to produce bio-oil. To this end, coconut husks were used as a medium for bio-oil production.

During the bio-oil production process, the ambient, surface, and internal temperature profiles of the carbonizer were monitored as shown in Figure 5. A few minutes after the biomass is ignited, the temperature inside the carbonizer increases over time to a maximum, then drops to a minimum before rising again. Initially, the temperature gradually rises to approximately 228°C, which is consistent with the dehydration of the biomass. During this phase, physically bound water is released as water vapor, along with oxygenated gases such as carbon monoxide (CO), carbon dioxide (CO_2), acetic acid (CH_3COOH), and methanol (CH_3OH) from the decomposition of the less stable components of biomass [15, 17]. At this stage, the bio-oil flow rate is relatively high, and the oil has a fairly clear appearance, indicating that this is indeed the dehydration stage. The bio-oil collected during this phase is expected to have a high-water content. From 228°C onwards, the temperature inside the furnace increases rapidly and almost linearly to its maximum value of 456°C (Tmax). The temperature fluctuations observed during this phase are likely attributable to the influence of wind. During this stage, an exothermic

Edelweiss Applied Science and Technology
ISSN: 2576-8484
Vol. 9, No. 5: 346-367, 2025
DOI: 10.55214/25768484.v9i5.6869

reaction occurs, with the thermal increase at Tmax possibly corresponding to the emission of combustion gases such as hydrogen (H_2), methane (CH_4), carbon monoxide (CO), carbon dioxide (CO_2), and volatile matter. These gases are produced as the combustion zone progresses, leading to local increases in heat as thermochemical reactions, such as pyrolysis and gasification, occur. This phenomenon has been previously documented by Homma, et al. [18]; Kisiki Nsamba, et al. [19] and Kongnine, et al. [20]. During this phase, the bio-oil collected exhibits a darker appearance and a moderate flow rate in comparison to the initial phase. Intermittently, viscous drops are also collected. This phase corresponds to the production of true bio-oil, a dark liquid with a smoky odor. The formation of bio-oil is attributed to the condensation of volatile substances emanating during the carbonization of biomass. It has been found to consist of complexes made up of approximately 300 main and minor organic compounds, including acids, alcohols, ketones, aldehydes, phenols, ethers, esters, sugars, furans, nitrogen compounds, and multifunctional compounds [15]. Within this temperature range, these compounds are released from the biomass in gaseous form. The augmentation of pressure within the chimney, in conjunction with a substantial residence time, results in the condensation of these gases, which are subsequently collected through an aperture in the carbonizer cover.

Subsequent to the combustion phase, a decline in temperature from Tmax to Tmin is observed, followed by an uptick. During this phase, the smoke emanating from the chimney undergoes a blue shift, signifying the culmination of the carbonation process. The subsequent rise in temperature is indicative of the combustion of the biochar produced. The liquid collected during this phase exhibits an appearance similar to that of the previous phase, but with a reduced flow rate as the drops become less frequent. This observation indicates that the level of volatile condensable matter has attained its limit, with the lignin a principal agent in the genesis of bio-oils having undergone complete decomposition [21, 22].

The external temperature, measured at the surface of the carbonizer, exhibits a similar trend to the internal temperature. However, it undergoes several fluctuations and displays lower values (as depicted by the red curve). These variations are attributed to the impact of wind and the presence of a layer of clay between the two coaxial cylinders, which functions as a thermal insulator. The differences between the maximum internal and external temperatures during the first two carbonization phases are 172°C and 392°C, respectively. These values reflect the attenuation of the temperatures of all the metal sheets and the clay layer, which contributed to the storage of heat. Furthermore, delays of 3 minutes and 24 minutes were observed between the maximum internal and external temperatures during the first two phases. These lag times are consistent with the minimum residence time required for effective fluid heating when employing carbonizers for co-production of hot water. The ambient air temperature was also recorded and is represented in Figure 3 by the black curve. The pattern exhibited by this curve differs significantly from the patterns observed in the other curves. It commenced at 37 °C, diminished to 28 °C, and then stabilized. The observed fluctuations are attributed to wind effects. The heat from the carbonizer had no effect on this temperature, as the thermocouple used to record it was placed 2 meters away from the carbonizer, a distance considered to be outside the zone of thermal radiation. The thermal decay of the environment is attributed to the movement of the Sun. Our carbonization sessions are initiated at approximately 2:00 pm to facilitate biomass desiccation, and the present session occurred on January 25, 2024, from 2:00 pm to 7:48 pm. Following sunset, the ambient air undergoes a process of moisture absorption and temperature decline, thereby contributing to the stabilization of the temperature.

Edelweiss Applied Science and Technology
ISSN: 2576-8484
Vol. 9, No. 5: 346-367, 2025
DOI: 10.55214/25768484.v9i5.6869

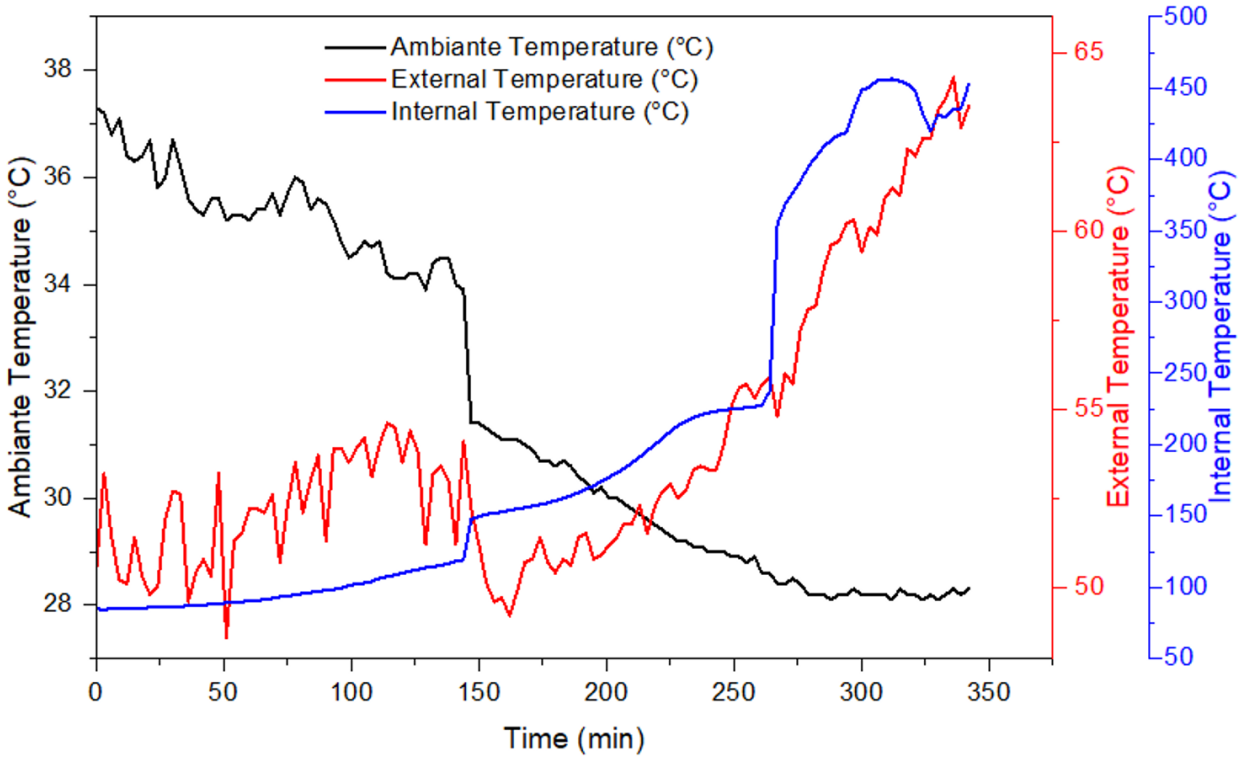

Figure 5.
Thermal profile during bio-oil production.

4.2. Influence of Maximum Carbonizations Temperature and Residence Time on Carbonization Yield

The present study investigated the influence of maximum temperature on the carbonization products of coconut shells, as illustrated in Figure 6. The data demonstrate a direct correlation between the bio-oil yield and the temperature, with an increase from 4.52% to 7.95% as the temperature rises from 414 °C to 445 °C. However, beyond 445 °C, a decline in the bio-oil yield is observed, with a decrease from 6.98% to 5.12% at higher temperatures. This finding suggests that the bio-oil yield attains its maximum at 445 °C. It is evident that the continuous increase in temperature beyond this optimum value has a substantial impact on the cracking behavior of volatile products. Conversely, the biochar yield exhibited a decline from 43.96% to 30.12% as the temperature increased from 414 °C to 456 °C. This observation indicates that the maximum temperature exerts a substantial influence on the decomposition of coconut shells into carbonization products.

These results are consistent with the literature [21, 23-27]. The cracking reaction that occurs during the carbonization process can break the C-C bonds into longer carbon chains of high molecular weight compounds, resulting in the formation of shorter carbon chains and lighter compounds. It has been demonstrated that as the temperature increases, the intensity of the cracking reaction also increases, leading to an increased yield of carbonization products. Specifically, at 445 °C, the primary decomposition of the biomass of the coconut shell is most pronounced, resulting in a higher production of volatile condensable matter. This increase is primarily due to the degradation of lignin, cellulose, and hemicellulose [28, 29] which contribute to the formation of tar. However, when the temperature exceeds its optimal value of 445°C, the bio-oil yield experiences a decline. This decline is attributed to the decomposition of volatiles into gaseous products and the subsequent breakdown of tar into gas and char. The secondary reaction causes the carbon chains of organic matter and hydrocarbons to break into shorter chains that cannot be condensed, leading to a reduced bio-oil yield [30].

Edelweiss Applied Science and Technology
ISSN: 2576-8484
Vol. 9, No. 5: 346-367, 2025
DOI: 10.55214/25768484.v9i5.6869

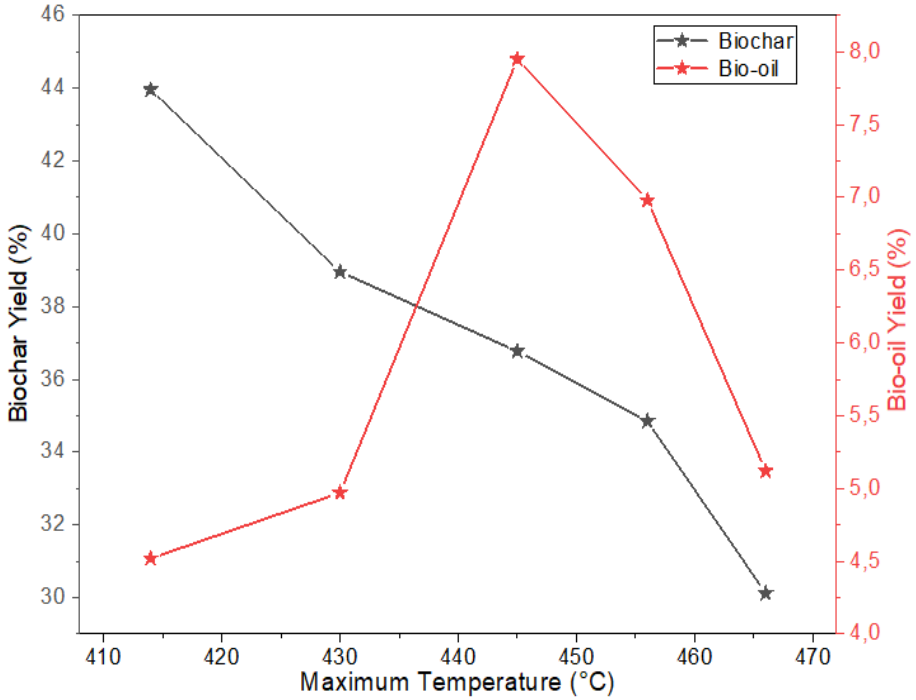

Figure 6.
Biochar and bio-oil Yields as function of maximum carbonization temperature.

In addition to the carbonization temperature, the residence time exerts a substantial influence on the yields of the carbonization products. As demonstrated in Figure 7, at a carbonization time of 365 minutes, the biochar and bio-oil yields are 43.96% and 4.52%, respectively. Conversely, an increase in the residence time leads to a shift in the yields toward higher values. Specifically, the bio-oil yield exhibits a maximum increase of 7.95% at a residence time of 435 minutes, while the biochar yield experiences a decrease to 30.12% for the same duration. This trend has also been observed by other researchers [24, 31]. The enhancement of bio-oil yield with an extended carbonization time can be attributed to the prolongation of chemical reactions, leading to an increased conversion of biomass into bio-oil. However, it is imperative to exercise caution with prolonged carbonization times, as excessively long durations can lead to over-degradation, which may compromise the quality of the bio-oil and result in the formation of undesirable by-products [24].

In addition to the yields of the carbonization products, the bio-oil ratio per kilogram of biomass is presented in the final column of Table 1. It is observed that this ratio peaks at 76.56 milliliters per kilogram when the bio-oil yield is at its highest. The lowest ratio of 44.61 ml/kg was observed and obtained at a carbonization temperature of 466 °C. The average bio-oil yield per kilogram of coconut shells was 57.03 ml.

Furthermore, the maximum biochar yield of 43.96% was achieved in our experiments at 414 °C, with an average yield of 37.30%. These yields are significantly higher than those reported by other researchers using the same biomass [23, 31] demonstrating the quality of the carbonization furnace and the efficiency of the method. Nevertheless, it is noteworthy that the maximum and average bio-oil yields obtained in this study remain lower than those reported in the extant literature [23, 26, 31, 32]. Consequently, further research is necessary to enhance the chimney carbonizer cover system, which functions as a bio-oil collection apparatus, with the objective of minimizing losses and optimizing bio-oil yields. The produced biochar from coconut shells in this study was preserved for subsequent processing into fuel briquettes, serving as an alternative fuel, as previously described in a study conducted in our laboratory [33].

Edelweiss Applied Science and Technology
ISSN: 2576-8484
Vol. 9, No. 5: 346-367, 2025
DOI: 10.55214/25768484.v9i5.6869

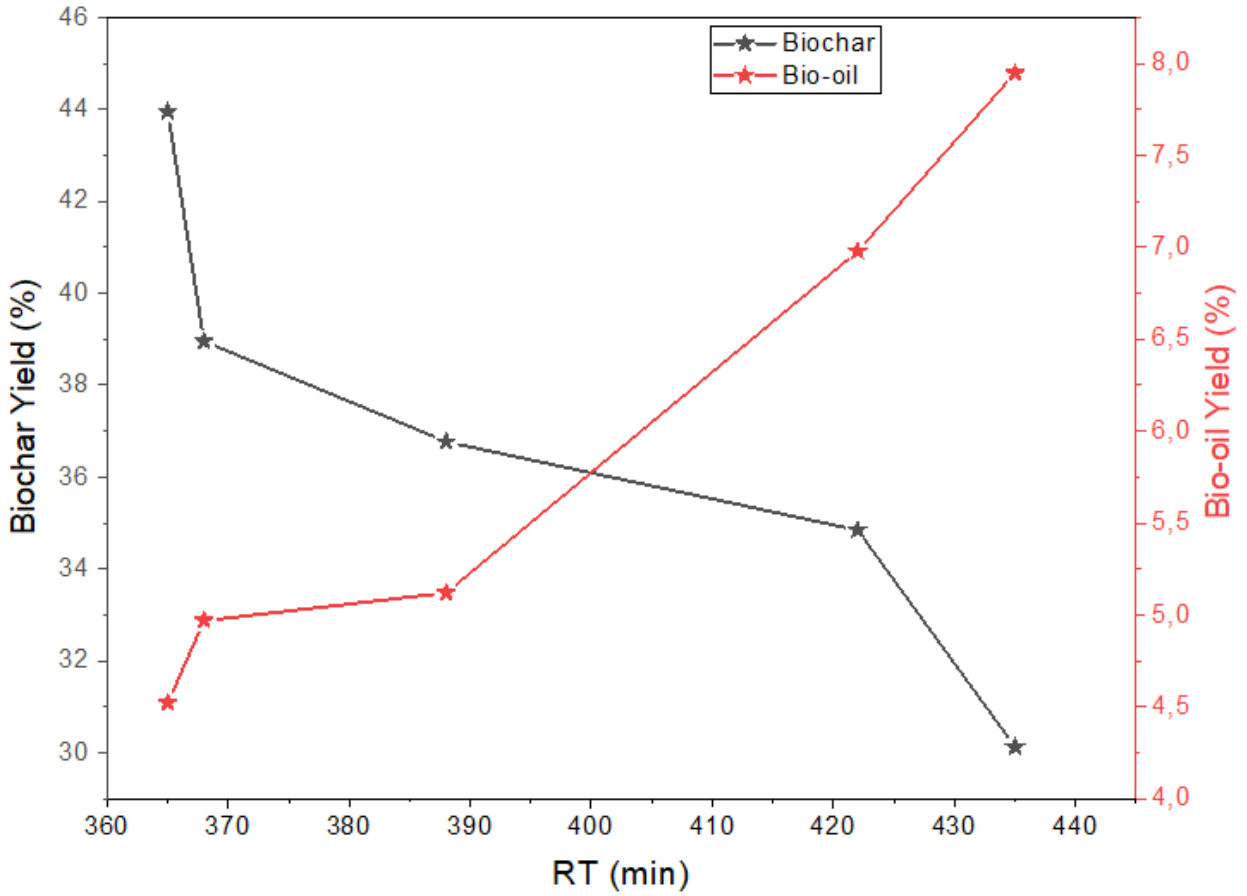

Figure 7.
Influence of Residence Time on product yields temperature

Table 1.
Maximum temperatures (Tmax), minimum temperatures (Tmin), Residence Time (RT), yield of biochar (Ybiochar), bio-oil (Ybio-oil) and the ratio of bio-oil per kilogram of biomass (Rbio-oil) during coconut shells carbonization.

Biomass	T_{max} (°C)	T_{min} (°C)	$Y_{biochar}$ (%)	$Y_{bio-oil}$ (%)	$R_{bio-oil}$ (ml/kg)
Coconut Shells	414	335	43.96	4.52	49.24
	430	368	38.96	4.97	49.45
	445	388	36.77	7.95	76.56
	456	422	34.85	6.98	66.37
	466	435	30.12	5.12	41.61
Average	-	-	37.30	5.58	57.03

4.3. Density of the produced bio-oil and bio-pitch

The bio-oil density, as deduced from the measurements, was found to be 1.05 g/cm^3. This density, which closely resembles that of water, suggests that the bio-oil is predominantly composed of water. After the heat treatment, a significant portion of the water present in the bio-oil evaporates, resulting in the formation of bio-pitch. The solution becomes viscous, and the heat treatment is terminated when the density reaches 1.30 g/cm^3, which is comparable to that of tar pitch [15].

Edelweiss Applied Science and Technology
ISSN: 2576-8484
Vol. 9, No. 5: 346-367, 2025
DOI: 10.55214/25768484.v9i5.6869

4.4. Electrode Elaboration Yield

The production of electrodes is a critical stage in our study, as it influences not only the efficiency of the molding process but also the optimal powder ratios to ensure strong adhesion between the binder and the powder. This stage involves the molding and demolding of the electrodes. A series of tests were conducted during this phase, and the production yields were calculated for each type of electrode, as presented in Table 2. Among the diverse samples, the pure neem biochar powder (B/T (1: 0)) exhibited the lowest yield at 14.29%. However, as the titanium oxide ratio increased, the yield also improved, reaching 100% for certain samples. This enhancement in yield can be ascribed to the malleability of the titanium oxide, which exhibited enhanced adhesion properties when compared to the pure biochar powder. This enhanced adhesion is likely a contributing factor to the observed increase in production yields with elevated titanium oxide content. The mean yield was 37.50%. This means that, of the 16 molded electrodes, only 6 can be demolded without breaking. Consequently, a thorough study of the molding system is imperative to enhance its efficiency. However, for powders containing a minimum of 33.33% titanium oxide, such as the B/T (2:1) sample, the mold achieves a yield of 100%.

Table 2.
Development yield.

Type of electrode	Elaboration yield (%)
B/T (1:0)	14.29
B/T (4:1)	20.00
B/T (2:1)	100.00
B/T (1:5)	100.00
Average	37.50

4.5. Electrode's Electrical Characteristics

In addition to the significance of the physical and chemical properties of the raw materials of the electrode performance, the ability of the bio-pitch to adhere to the particles of the neem charcoal powder, considered as coke, also plays a crucial role in determining the properties of the annealed electrodes. Consequently, bio-pitch was employed in the fabrication of the electrode paste. The performance of an electrode is closely linked to its electrochemical properties. To assess the potential of the developed electrodes as alternatives in biofuel cells, they were characterized alongside a graphite electrode used as a reference. This characterization entailed the determination of the apparent density, electrical resistivity, and other electrochemical properties of each electrode using electrochemical impedance spectroscopy (EIS).

4.6. Density of the Produced Electrodes

The results of the electrode density measurements are displayed as histograms in Figure 8. For each type of electrode, the density of the non-annealed electrodes is higher than that of the annealed electrodes. During the annealing process, the binder matrix (bio-pitch) samples experienced a substantial loss in total mass, likely attributable to the volatilization of the binder's light fractions. The electrodes fabricated from pure neem charcoal (B/T (1:0)) exhibited the lowest densities, measuring 1.42 g/cm^3 and 1.21 g/cm^3 for the raw and annealed electrodes, respectively.

Edelweiss Applied Science and Technology
ISSN: 2576-8484
Vol. 9, No. 5: 346-367, 2025
DOI: 10.55214/25768484.v9i5.6869

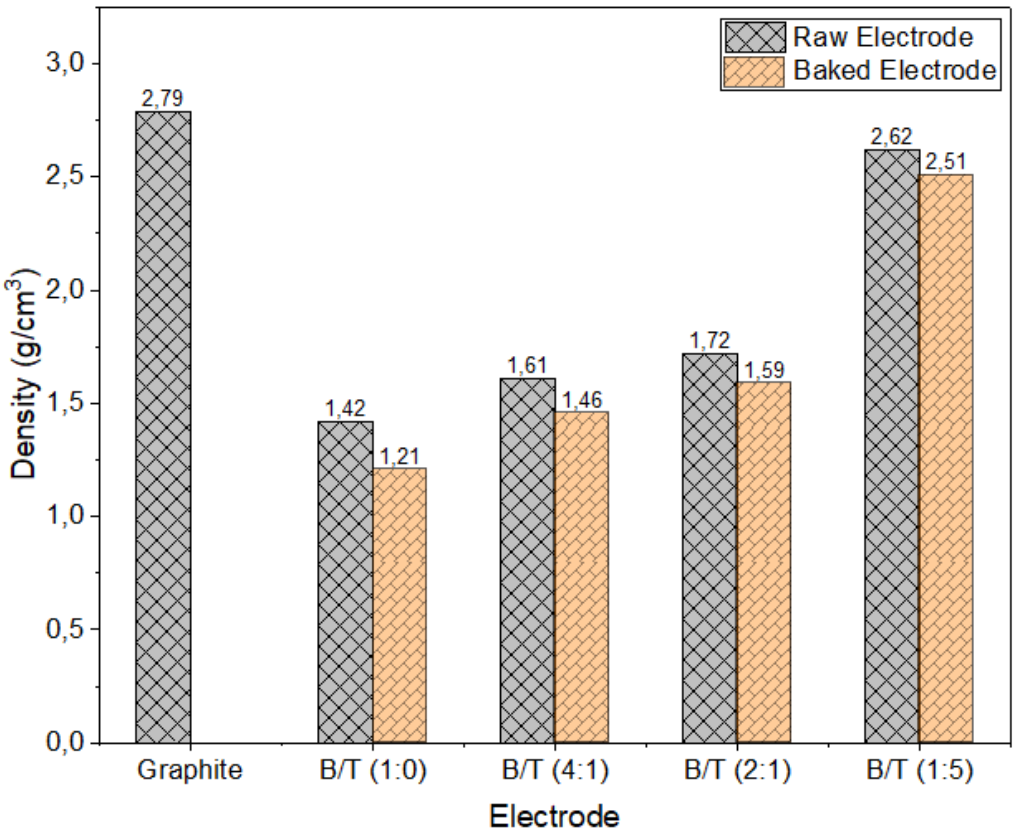

Figure 8.
Density of Raw and Annealed Electrodes Produced.

In contrast, the highest recorded density values for the non-annealed and annealed electrodes were 2.62 g/cm³ and 2.51 g/cm³, respectively, obtained with a B/T ratio of 1:5. In comparison to the graphite electrode, which has a density of 2.79 g/cm³, these values are lower. This difference can be ascribed to the manufacturing technique employed for the graphite electrode, particularly the compaction process and the annealing temperature.

The incorporation of titanium oxide into the neem charcoal powder has been found to exert a substantial influence on the density of the resulting electrodes. The density of the electrodes increases with the titanium oxide content in the sample, irrespective of whether the electrodes are non-annealed or annealed. This increase in electrode density can be attributed to the higher density of titanium oxide compared to biochar powder (4.24 g/cm³ versus 0.52 g/cm³) and the modification of the biochar powder surface structure, which enhances its wettability with bio-pitch. This enhanced wettability facilitates the diffusion of bio-pitch into the inter- and intra-particle pores, consequently reducing the electrode's porosity. It is widely acknowledged that an increased electrode density is advantageous, as it prolongs the lifespan of the carbon within the electrode and, consequently, the overall lifespan of the electrode. However, if the electrode density becomes excessively high, it may result in cracking during the annealing process due to the substantial release of volatile compounds [34].

The release of volatiles compounds during the annealing process has been shown to result in both mass loss and volume shrinkage of the electrodes, as outlined in Table 3. The B/T (1:0) sample demonstrates the most substantial mass loss, reaching 56.25%, and a volume shrinkage of 40.60%. For B/T (4:1), the mass loss and shrinkage are 18.18% and 9.98%, respectively, while for B/T (2:1), these values are 30.65% and 25.16%. The lowest mass loss and shrinkage are observed in the B/T (1:5)

Edelweiss Applied Science and Technology
ISSN: 2576-8484
Vol. 9, No. 5: 346-367, 2025
DOI: 10.55214/25768484.v9i5.6869

sample, with values of 6.25% and 2.05%, respectively. These results suggest a direct correlation between higher volume shrinkage and greater mass loss, which in turn affects the density of electrodes after annealing. The capacity of the non-annealed electrode to undergo shrinkage during the annealing process suggests that there is adequate adhesion between the bio-pitch and the fine particles present in the powder samples. In annealed electrodes, the combination of neem charcoal particles and bio-pitch functions as a conductor. This combination may induce low electrical resistivity in the electrodes, given that the electrical resistivity of carbonaceous materials is largely dependent on the degree of graphitization achieved by the heat treatment [35].

Table 3.
Mass Loss and Volume shrinkage of Produced Electrodes.

Electrode	Mass Loss (%)	Volume shrinkage (%)
B/T (1:0)	56.25	40.60
B/T (4:1)	18.18	9.98
B/T (2:1)	30.65	25.16
B/T (1:5)	6.25	2.05

4.7. Electrical Resistivity Decreasing with Titanium Oxide Addition

Resistivity is a fundamental parameter that determines the quality of an electrode. It provides insight into the mobility of charge carriers within the conductor (electrode). It is important to note that resistivity is inversely proportional to both the density and mobility of the charge carriers [36].

Table 4 presents the resistivity values of the various electrodes that were tested. As demonstrated in this Table, irrespective of the electrode type, the resistivity of annealed electrodes is consistently lower than that of non-annealed electrodes. The reduction in resistivity after annealing varies slightly depending on the electrode type: Specifically, it was observed to be 98.31% for B/T (1:0), 99.64% for B/T (4:1), 99.88% for B/T (2:1), and 100% for B/T (1:5). This substantial decline in resistivity signifies that annealing exerts a considerable influence on the electrical resistivity of the electrodes. This phenomenon is likely facilitated by the heat treatment process, which allows for the penetration of the pitch into the electrode's pores, thereby reducing porosity and, consequently, resistivity. Furthermore, the elevated temperature may facilitate the volatilization of specific insulating impurities present in the electrode, thereby enhancing the efficacy of the heat treatment process. The present study observed a decrease in resistivity of approximately 0.1% per degree Celsius. For the non-annealed electrodes, B/T (1:0) exhibited the lowest electrical resistivity of 4.40×10^{-2} Ω.m, while the other non-annealed electrodes exhibited higher electrical resistivity, which increased with the titanium oxide content. This observation indicates that the incorporation of titanium oxide may result in the formation of porosity within the raw electrodes. Additionally, given the nature of TiO_2 P25 as a semiconductor, its incorporation into the samples results in enhanced electrical insulating properties of the electrodes. However, after annealing, the trend is reversed. This may be due not only to the removal of insulating impurities during annealing, but more importantly to the formation of more conductive compounds such as Ti_2O_3, Ti_3O_5 and TiC [37, 38]. Except for B/T (1:5), the electrical resistivity of the annealed electrodes decreases with increasing titanium oxide content. This indicates that titanium oxide enhances the ability of bio-pitch to penetrate into the micropores during heat treatment. Among the developed electrodes, the baked B/T (2:1) electrode has the lowest resistivity at 4.28×10^{-4} Ω.m. Although this value is approximately 9.3 times higher than the resistivity of a graphite electrode tested under the same conditions, the difference is attributed to both the nature of the raw materials and the processing conditions, particularly the densification and heat treatment. For example, the graphite electrode was treated at a much higher temperature than 2000 °C [39].

Edelweiss Applied Science and Technology
ISSN: 2576-8484
Vol. 9, No. 5: 346-367, 2025
DOI: 10.55214/25768484.v9i5.6869

Table 4.
Resistivity of elaborated electrodes.

Electrode	Resistivity (Ω.m)		Decay rate (%)
	Raw Electrode	Annealed Electrode	
Graphite	4.58 x 10 $^{-5}$	-	-
B/T (1:0)	4.40 x 10 $^{-2}$	7.45 x 10 $^{-4}$	98.31
B/T (4:1)	1.36 x 10 $^{-1}$	4.93 x 10 $^{-4}$	99.64
B/T (2:1)	3.45 x 1 0 $^{-1}$	4.28 x 10 $^{-4}$	99.88
B/T (1:5)	1.80 x 10 ^{6}	1.37 x 10 $^{-2}$	100.00

4.8. Electrochemical Impedance Spectroscopy Analysis of the Electrodes

In order to investigate the electrochemical properties and behavior of the electrode/electrolyte interface, some of the studied electrodes were characterized by electrochemical impedance spectroscopy (EIS). However, due to the friability of the B/T (1:0) and B/T (4:1) electrodes after annealing, these could not be characterized by EIS. Consequently, the characterization was confined to two annealed electrodes (B/T (2:1) and B/T (1:5)) along with the graphite electrode. The results of the electrochemical impedance spectroscopy tests are presented in Figure 9. As demonstrated in this Figure, the Nyquist plots of the three electrodes are analogous, each exhibiting a sloping line (Figure 9a). The intersection points of the EIS curves with the x-axis reveal that the studied electrodes possess low series resistances for a given surface area. This resistance is defined as the sum of the resistances of the solution, the connecting wires, and the tested electrode. The series resistance for the graphite electrode is 1.652 Ω.cm^2, while those for the B/T (2:1) and B/T (1:5) electrodes are 1.513 Ω.cm^2 and 3.028 Ω.cm^2, respectively. A comparison of the B/T (2:1) electrode with graphite reveals that the former exhibits a lower resistance, indicative of an enhanced electron transfer rate. According to the extant literature, a high electron transfer rate is associated with low ohmic resistance of the electrode [40, 41]. However, the B/T (1:5) electrode exhibited a resistance that was 1.8 times greater than that of graphite, indicating that the incorporation of titanium oxide into the biochar powder substantially impacts the electrochemical properties of the electrodes.

In order to ascertain the remaining electrical parameters of the electrodes under operating conditions, the fitting method was utilized for analyzing the EIS data with equivalent circuits. The Zview software was utilized for the simulations, and three simple equivalent circuits were examined for each electrode type. The optimal circuit for each electrode was selected based on the mechanisms suggested by the Nyquist curves and the error rates associated with each model [41-45]. The optimized equivalent circuits and their corresponding electrical parameters are presented in Table 5. Within this table, the series resistance, Rs, signifies the resistance posed by the connecting wires, the tested electrode, and the electrolyte (sodium sulfate) between the working electrode and the reference electrode. Beyond this resistive impedance, other electrical components were considered, including L, a purely inductive element that accounts for the contribution of wound wires or electrical connections at high frequencies and degradation processes at low frequencies; Rct, the charge transfer resistance; Cdl or CPE, which denotes the double layer capacitance; and Ws, the finite Warburg impedance associated with the diffusion phenomenon that can be attributed to redox processes [14, 46]. The graphite and B/T (2:1) electrodes exhibit an ideal double layer capacitance, whereas the B/T (1:5) electrode displays a non-ideal capacitance modeled by a constant phase element (CPE). This discrepancy is likely attributable to the inhomogeneity and porosity of the B/T (1:5) electrode surface. The charge transfer resistance Rct is directly linked to the number of catalytic sites available for the reduction reactions. A lower Rct value is indicative of a greater number of catalytic sites. As demonstrated in Table 5, the Rct values for the B/T (2:1) and B/T (1:5) electrodes are 3.3 and 59.8 times lower, respectively, than that of the graphite electrode. This finding indicates that the electrodes developed in this study exhibit a significantly higher capacity for reducing and storing electrical energy in comparison to the graphite electrode. The enhanced performance can be attributed to several factors: the presence of TiO_2, which

Edelweiss Applied Science and Technology
ISSN: 2576-8484
Vol. 9, No. 5: 346-367, 2025
DOI: 10.55214/25768484.v9i5.6869

improves the catalytic properties of the electrodes; the quality of the bio-pitch, which promotes strong bonding between the TiO_2 particles and the biochar, as well as good adhesion between the different powder particles; and the effectiveness of the development method used in this study. Considering the total surface area of each electrode, the Rs values are 18.85 Ω for the graphite electrode, 21.46 Ω for the B/T (2:1) electrode and 35.03 Ω for B/T (1:5) electrode. The graphite electrode exhibits the lowest Rs value, attributable to its low resistivity, as determined through the four-point method. In regard to charge transfer, the Rct values are 15.47 Ω for the graphite electrode, 6.16 Ω for the B/T (2:1) electrode, and 0.25 Ω for the B/T (1:5) electrode. This outcome lends further credence to the hypothesis that the addition of TiO_2 to the biochar powder significantly enhances the electrical properties of the electrodes.

An analysis of the equivalent circuits reveals that, following its passage through the resistor Rs and the inductor L, the current takes one of two possible paths, depending on the frequency (pulsation). At low frequencies, the current flows through Rct, whereas at high frequencies, it favors the path containing the double layer capacitance. The diffusion parts (Ws), with the same exponential factor (Ws-P=0.5), exhibit significantly lower diffusion impedances (Ws-R) in comparison to graphite. Conversely, the diffusion time (Ws-T) of these electrodes exceeds that of graphite. This finding indicates that the thickness of the graphite electrode's diffusion layer is reduced.

Utilizing the EIS data, we have plotted the impedance modulus of each electrode, resulting in Bode plots (see Figure 9b). These plots demonstrate that the impedance modulus of the developed composite electrodes is significantly lower than that of the graphite electrode at low and medium frequencies. However, at very high frequencies, the graphite electrode impedance becomes slightly lower. Among the developed electrodes, the B/T (2:1) electrode demonstrates the lowest impedance modulus. In a similar manner, the phase angle plots (Figure 9c) demonstrate that the impedance of the developed composite electrodes is lower than that of the graphite electrode. A phase shift angle close to -90° corresponds to higher capacitance, while a phase shift angle near to 0° indicates a higher resistance [14]. Consequently, the B/T composite electrodes developed in this study, due to their low impedance, are more suitable for enhanced electricity recovery in biofuel cells.

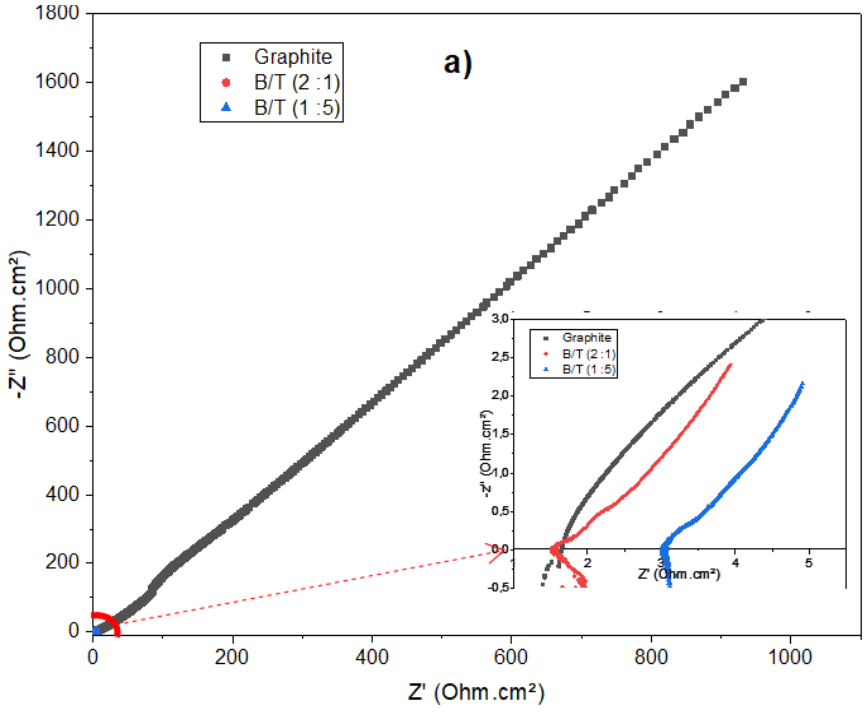

Edelweiss Applied Science and Technology
ISSN: 2576-8484
Vol. 9, No. 5: 346-367, 2025
DOI: 10.55214/25768484.v9i5.6869

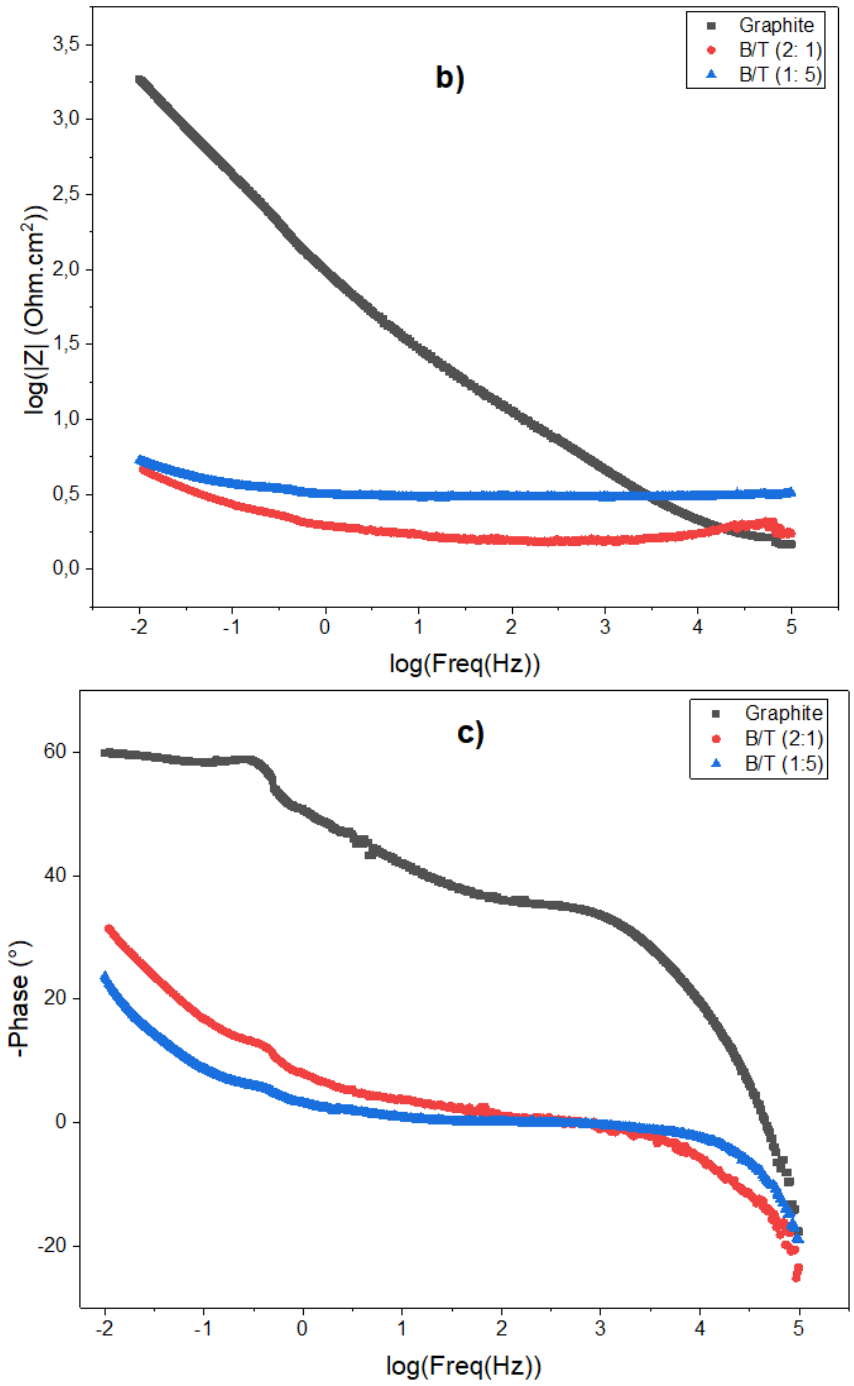

Figure 9.
Electrochemical Impedance Spectroscopy Curves: a) Nyquist plot b) and c) Bode Plot.

Edelweiss Applied Science and Technology
ISSN: 2576-8484
Vol. 9, No. 5: 346-367, 2025
DOI: 10.55214/25768484.v9i5.6869

Table 5.
Electrical Parameters of studied electrodes.

Electrode	Circuit Equivalent		Rs ($\Omega.cm^2$)	Rct ($\Omega.cm^2$)	L ($\mu H.cm^2$)	C_{dl} ($F.cm^2$)	CPE-T ($F.cm^2$)	CPE-P ($F.cm^2$)	Ws-R ($\Omega.cm^2$)	Ws-T (s)	Ws-P
Graphite	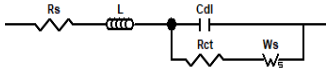	Value	1.652	1.315	87.759	1.276×10^{-5}	-	-	91.35	7.130×10^{-5}	0.5
		Error (%)	0.40	5.63	2.45	2.04	-	-	1.94	7.04	-
B/T (2:1)	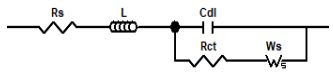	Value	1.513	0.394	1254.9	0.017	-		0.259	0.159	0.5
		Error (%)	0.14	0.59	3.10	1.52	-	-	2.53	3.13	-
B/T (1:5)	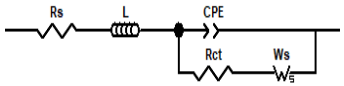	Value	3.028	0.022	1.732	-	7.305×10^{-9}	0.752	3.52×10^{-4}	0.123	0.5
		Error (%)	0.30	7.91	1.57	-	18.27	6.92	6.40	8.99	-

Edelweiss Applied Science and Technology
ISSN: 2576-8484
Vol. 9, No. 5: 346-367, 2025
DOI: 10.55214/25768484.v9i5.6869

5. Conclusion

In this study, composite electrodes were developed using biochar powder (feedstock) derived from the carbonization of neem wood and titanium oxide at various levels. Bio-pitch, derived from the carbonization of coconut shells, was employed as a binding agent to agglomerate the powder. The electrodes were formed, compacted, and demolded using a cylindrical mold that was fabricated during the study. Following this, the electrodes underwent a heat treatment in an oven. The characterization of the resulting electrodes, in conjunction with a graphite electrode serving as a reference, facilitated the determination of their electrical and electrochemical properties. The results of this study revealed that electrode density increases with the TiO_2 content. The density ranges from 1.42 g/cm^3 and 1.21 g/cm^3 for B/T (1:0) raw and annealed electrodes, respectively, to 2.62 g/cm^3 and 2.51 g/cm^3 for B/T (1:5) raw and annealed electrodes, respectively. The graphite electrode exhibited the highest density at 2.79 g/cm^3. The four-point method for resistivity measurement indicated that, with the exception of B/T (1:5), the resistivity of the raw and annealed electrodes varies inversely with TiO_2 content. The annealed B/T (2:1) electrode exhibited the lowest resistivity at 4.28 x 10^{-4} Ω.m, and the graphite electrode demonstrated a resistivity value that was 9.3 times lower. Furthermore, the electrochemical analysis revealed that, in addition to their low impedance, the developed composite electrodes exhibited charge transfer resistances (Rct) that were significantly lower than those of the graphite electrode. Specifically, the Rct values for the B/T (2:1) and B/T (1:5) electrodes were recorded as 6.16 Ω and 0.25 Ω, respectively, in comparison to the 15.47 Ω value observed for the graphite electrode. These results suggest that using biochar instead of fossil coal and valorization of coconut shells into bio-pitch instead of fossil pitch is a more sustainable and effective approach for producing high-performance electrodes. These electrodes are particularly suitable for efficient energy recovery in low power systems such as biofuel-cells.

Funding:

The work was supported by funding from the World Bank for the project "Centre d'Excellence Régional pour Mastery of Electricity (CERME)" of Universty of Lomé (Crédit IDA 6512-TG; Don IDA 536IDA).

Author Contribution Statement:

N'Gissa ATTAH: Conceptualization, experimental manipulations, data management, formal analysis, writing - original version, Damgou KONGNINE MANI: Project management, methodology, general supervision and validation, Essowè MOUZOU: Methodology, experimental supervision (EIS), writing - revision and Pali KPELOU: Methodology, experimental supervision (heat treatment and resistivity determination), writing - revision.

Transparency:

The authors confirm that the manuscript is an honest, accurate, and transparent account of the study; that no vital features of the study have been omitted; and that any discrepancies from the study as planned have been explained. This study followed all ethical practices during writing.

References

[1] H. Song, S. Zhang, X. Long, X. Yang, H. Li, and W. Xiang, "Optimization of bioelectricity generation in constructed wetland-coupled microbial fuel cell systems," *Water*, vol. 9, no. 3, p. 185, 2017. https://doi.org/10.3390/w9030185

[2] Q. Wu, J. Liu, Q. Li, W. Mo, R. Wan, and S. Peng, "Effect of electrode distances on remediation of eutrophic water and sediment by sediment microbial fuel cell coupled floating beds," *International Journal of Environmental Research and Public Health*, vol. 19, no. 16, p. 10423, 2022. https://doi.org/10.3390/ijerph191610423

[3] L. Doherty, X. Zhao, Y. Zhao, and W. Wang, "The effects of electrode spacing and flow direction on the performance of microbial fuel cell-constructed wetland," *Ecological Engineering*, vol. 79, pp. 8-14, 2015. http://dx.doi.org/10.1016/j.ecoleng.2015.03.004

[4] K. You, Z. Zhou, C. Gao, and Q. Yang, "One-step preparation of biochar electrodes and their applications in sediment microbial electrochemical systems," *Catalysts*, vol. 11, no. 4, p. 508, 2021. https://doi.org/10.3390/catal11040508

[5] A. Kumar *et al.*, "Application of biogenic TiO2 nanoparticles as ORR catalysts on cathode for enhanced performance of microbial fuel cell," *Catalysts*, vol. 13, no. 6, p. 937, 2023. https://doi.org/10.3390/catal13060937

[6] A. A. Yaqoob, M. N. M. Ibrahim, and K. Umar, "Biomass-derived composite anode electrode: Synthesis, characterizations, and application in microbial fuel cells (MFCs)," *Journal of Environmental Chemical Engineering*, vol. 9, no. 5, p. 106111, 2021. https://doi.org/10.1016/j.jece.2021.106111

[7] F.-Y. Lin *et al.*, "Trapa natans husk-derived carbon as a sustainable electrode material for plant microbial fuel cells," *Applied Energy*, vol. 325, p. 119807, 2022. https://doi.org/10.1016/j.apenergy.2022.119807

[8] K. Sonu, M. Sogani, Z. Syed, J. Rajvanshi, and S. C. Pandey, "Performance evaluation of Epipremnum aureum plant-based microbial fuel cell using composite anode made up of carbonized corncob and carbon rod," *Biomass Conversion and Biorefinery*, vol. 14, no. 4, pp. 5149-5156, 2024. https://doi.org/10.1007/s13399-022-02794-6

[9] A. A. Yaqoob, M. N. M. Ibrahim, and C. Guerrero-Barajas, "Modern trend of anodes in microbial fuel cells (MFCs): an overview," *Environmental technology & innovation*, vol. 23, p. 101579, 2021. https://doi.org/10.1016/j.eti.2021.101579

[10] A. A. Yaqoob, M. N. M. Ibrahim, A. S. Yaakop, and M. Rafatullah, "Utilization of biomass-derived electrodes: a journey toward the high performance of microbial fuel cells," *Applied Water Science*, vol. 12, no. 5, p. 99, 2022. https://doi.org/10.1007/s13201-022-01632-4

[11] F. Yu, C. Wang, and J. Ma, "Applications of graphene-modified electrodes in microbial fuel cells," *Materials*, vol. 9, no. 10, p. 807, 2016. https://doi.org/10.3390/ma9100807

[12] M. Z. Iqbal, S. Siddique, A. Khan, S. S. Haider, and M. Khalid, "Recent developments in graphene based novel structures for efficient and durable fuel cells," *Materials Research Bulletin*, vol. 122, p. 110674, 2020. https://doi.org/10.1016/j.materresbull.2019.110674

[13] A. Hussein, M. Fafard, D. Ziegler, and H. Alamdari, "Effects of charcoal addition on the properties of carbon anodes," *Metals*, vol. 7, no. 3, p. 98, 2017. https://doi.org/10.3390/met7030098

[14] C. H. Yen, S.-H. Chuang, R.-Y. Huang, P.-I. Liu, M.-C. Chang, and R.-Y. Horng, "Titanium dioxide/activated carbon electrode with polyurethane binder for the removal of indium ions via capacitive deionization," *Processes*, vol. 9, no. 8, p. 1427, 2021. https://doi.org/10.3390/pr9081427

[15] Y. Lu, "Interaction of bio-pitch with coke: Effect of bio-pitch on anode formulation," Unpublished Master's Thesis. Université de Québec, Canada., 2020.

[16] P. Kpelou, D. M. Kongnine, R. Asse, and E. Mouzou, "Experimental investigation of hot water cogeneration using a carbonizer fit out with a preheating system," *International Journal of Low-Carbon Technologies*, vol. 17, pp. 327-332, 2022. https://doi.org/10.1093/ijlct/ctac003

[17] ASTM D5502-00, *Standard test method for apparent density by physical measurements of manufactured anode and cathode carbon used by the aluminum industry*. ASTM International. https://doi.org/10.1520/D5502-00, 2000.

[18] H. Homma, H. Homma, and M. Idris, "Wood pyrolysis in pre-vacuum chamber," *Journal of Sustainable Bioenergy Systems*, vol. 3, no. 04, p. 243, 2013. https://doi.org/10.4236/jsbs.2013.34033

[19] H. Kisiki Nsamba, S. E. Hale, G. Cornelissen, and R. T. Bachmann, "Sustainable technologies for small-scale biochar production—a review," *Journal of Sustainable Bioenergy Systems*, vol. 5, no. 1, pp. 10–31, 2015. https://doi.org/10.4236/jsbs.2015.51002

[20] D. M. Kongnine, P. Kpelou, K. Sodoga, and K. Napo, "Evaluation of some combustion characteristics of biochar produced from coconut husks, corn cobs and palm kernel shells," *International Journal of Innovation and Applied Studies*, vol. 24, no. 3, pp. 1124-1130, 2018.

[21] S. Jamilatun, Y. Elisthatiana, S. N. Aini, I. Mufandi, and A. Budiman, "Effect of temperature on yield product and characteristics of bio-oil from pyrolysis of Spirulina platensis residue," *Elkawnie*, vol. 6, no. 1, pp. 96-108, 2020. https://doi.org/10.22373/ekw.v6i1.6323

[22] K. M. Qureshi, A. N. K. Lup, S. Khan, F. Abnisa, and W. M. A. W. Daud, "Effect of temperature and feed rate on pyrolysis oil produced via helical screw fluidized bed reactor," *Korean Journal of Chemical Engineering*, vol. 38, pp. 1797-1809, 2021. https://doi.org/10.1007/s11814-021-0842-0

Edelweiss Applied Science and Technology
ISSN: 2576-8484
Vol. 9, No. 5: 346-367, 2025
DOI: 10.55214/25768484.v9i5.6869

[23] J. K. Sarkar and Q. Wang, "Different pyrolysis process conditions of South Asian waste coconut shell and characterization of gas, bio-char, and bio-oil," *Energies*, vol. 13, no. 8, p. 1970, 2020. https://doi.org/10.3390/en13081970

[24] L. Maulinda *et al.*, "The influence of pyrolysis time and temperature on the composition and properties of bio-oil prepared from tanjong leaves (Mimusops elengi)," *Sustainability*, vol. 15, no. 18, p. 13851, 2023. https://doi.org/10.3390/su151813851

[25] B. D. Afrah, M. I. Riady, P. Payomthip, R. V. Ramadhanty, F. Rizki, and M. L. Alfayyadh, "Analysis of liquid smoke grade characteristics from coconut shells and palm kernel shell waste through a slow pyrolysis process," *Journal of Engineering and Technological Sciences*, vol. 56, no. 4, pp. 545-558, 2024.

[26] Y. Gao, Y. Yang, Z. Qin, and Y. Sun, "Factors affecting the yield of bio-oil from the pyrolysis of coconut shell," *SpringerPlus*, vol. 5, pp. 1-8, 2016. https://doi.org/10.1186/s40064-016-1974-2

[27] M. Joardder, M. R. Islam, and M. R. A. Beg, "Pyrolysis of coconut shell for bio-oil," in *Proceedings of the 9th International Conference on Mechanical Engineering*, 2011.

[28] W. A. Rizal *et al.*, "Chemical composition of liquid smoke from coconut shell waste produced by SME in Rongkop Gunungkidul," presented at the IOP Conference Series: Earth and Environmental Science, IOP Publishing, 2020.

[29] S. Husseinsyah and M. Mostapha, "The effect of filler content on properties of coconut shell filled polyester composites," *Malaysian Polymer Journal*, vol. 6, no. 1, pp. 87-97, 2011.

[30] L. Maulinda *et al.*, "Effects of temperature and times on the product distribution of bio-oils derived from Typha latifolia pyrolysis as renewable energy," *Results in Engineering*, vol. 18, p. 101163, 2023. https://doi.org/10.1016/j.rineng.2023.101163

[31] R. G. Bhad, S. R. Sedani, and S. N. Dongerdive, "Pyrolysis of coconut shell to produce crude oil," *South Asian Journal of Food Technology and Environment*, vol. 6, no. 1, pp. 917-922, 2020. https://doi.org/10.46370/sajfte.2020.v06i01.06

[32] A. Amrullah and S. E. Teguh, "Coconut shell bio-oil distillation: Its characteristic and product distribution," presented at the IOP Conference Series: Earth and Environmental Science, 2022.

[33] P. Kpelou, D. M. Kongnine, S. Kombate, E. Mouzou, and K. Napo, "Energy efficiency of briquettes derived from three agricultural waste's charcoal using two organic binders," *Journal of Sustainable Bioenergy Systems*, vol. 9, no. 02, pp. 79–89, 2019. https://doi.org/10.4236/jsbs.2019.92006

[34] B. Amara, D. Kocaefe, Y. Kocaefe, D. Bhattacharyay, J. Côté, and A. Gilbert, "Partial replacement of petroleum coke with modified biocoke during production of anodes used in the aluminum industry: Effect of additive type," *Applied Sciences*, vol. 12, no. 7, p. 3426, 2022. https://doi.org/10.3390/app12073426

[35] A. Hussein, D. Picard, and H. Alamdari, "Biopitch as a binder for carbon anodes: Impact on carbon anode properties," *ACS Sustainable Chemistry & Engineering*, vol. 9, no. 12, pp. 4681-4687, 2021. https://doi.org/10.1021/acssuschemeng.1c00618

[36] Y. Singh, "Electrical resistivity measurements: A review," *International Journal of Modern Physics: Conference Series*, vol. 22, pp. 745–756, 2013. https://doi.org/10.1142/S2010194513010970

[37] T. Lv, F. Tian, and T. Hu, "Preparation of titanium carbide by carburisation of titanium dioxide," *Processes*, vol. 12, no. 1, p. 102, 2024. https://doi.org/10.3390/pr12010102

[38] L.-M. Berger, W. Gruner, E. Langholf, and S. Stolle, "On the mechanism of carbothermal reduction processes of TiO2 and ZrO2," *International Journal of Refractory Metals and Hard Materials*, vol. 17, no. 1-3, pp. 235-243, 1999. https://doi.org/10.1016/S0263-4368(98)00077-8

[39] J. Zhang, J. Li, D. Ye, X. Zhu, Q. Liao, and B. Zhang, "Tubular bamboo charcoal for anode in microbial fuel cells," *Journal of Power Sources*, vol. 272, pp. 277-282, 2014. https://doi.org/10.1016/j.jpowsour.2014.08.115

[40] A. A. Yaqoob, M. N. M. Ibrahim, A. S. Yaakop, K. Umar, and A. Ahmad, "Modified graphene oxide anode: a bioinspired waste material for bioremediation of Pb2+ with energy generation through microbial fuel cells," *Chemical Engineering Journal*, vol. 417, p. 128052, 2021. https://doi.org/10.1016/j.cej.2020.128052

[41] Y.-H. Hung, T.-Y. Liu, and H.-Y. Chen, "Renewable coffee waste-derived porous carbons as anode materials for high-performance sustainable microbial fuel cells," *ACS Sustainable Chemistry & Engineering*, vol. 7, no. 20, pp. 16991-16999, 2019. https://doi.org/10.1021/acssuschemeng.9b02405

[42] H. M. Abd El-Lateef, M. M. Khalaf, V.-D. Dao, and I. M. Mohamed, "Electrochemical impedance investigation of dye-sensitized solar cells based on electrospun TiO2 nanofibers photoanodes," *Materials*, vol. 15, no. 17, p. 6175, 2022. https://doi.org/10.3390/ma15176175

[43] V.-D. Dao and H.-S. Choi, "Balance between the charge transfer resistance and diffusion impedance in a CNT/Pt counter electrode for highly efficient liquid-junction photovoltaic devices," *Organic Electronics*, vol. 58, pp. 159-166, 2018. https://doi.org/10.1016/j.orgel.2018.03.046

[44] I. M. Mohamed and C. Liu, "Chemical design of novel electrospun CoNi/Cr nanoparticles encapsulated in C-nanofibers as highly efficient material for urea oxidation in alkaline media," *Applied Surface Science*, vol. 475, pp. 532-541, 2019. https://doi.org/10.1016/j.apsusc.2019.01.003

[45] F. Guo *et al.*, "Electrochemical impedance analysis of urea electro-oxidation mechanism on nickel catalyst in alkaline medium," *Electrochimica Acta*, vol. 210, pp. 474-482, 2016. https://doi.org/10.1016/j.electacta.2016.05.149

[46] J. Lim, S. Y. Ryu, J. Kim, and Y. Jun, "A study of TiO 2/carbon black composition as counter electrode materials for dye-sensitized solar cells," *Nanoscale Research Letters*, vol. 8, pp. 1-5, 2013. https://doi.org/10.1186/1556-276X-8-227

Edelweiss Applied Science and Technology
ISSN: 2576-8484
Vol. 9, No. 5: 346-367, 2025
DOI: 10.55214/25768484.v9i5.6869